the case of uniaxial strain, a deviation of up to 5% occurs, but it becomes small for $\theta = 0$ and 90 deg. The deviation can be seen to be strongly dependent on the state of strain.

The maximum relative deviation in ψ for any particular lay-up can be obtained by extremizing the ratio $\lambda = \psi_{se}/\psi_{cm}$. This results in the eigenvalue problem

$$\left(\begin{bmatrix} A'' & B'' \\ B'' & D'' \end{bmatrix}_{se} - \lambda \begin{bmatrix} A'' & B'' \\ B'' & D'' \end{bmatrix}_{cm} \right) \begin{Bmatrix} \epsilon_m \\ \kappa \end{Bmatrix} = 0 \qquad (23)$$

where the double primed quantities are the imaginary part of the (complex) stiffness matrices A^*, B^*, and D^* of classical laminated plate theory,[2] and ϵ_m and κ are the amplitudes of the cyclic midplane strains and curvatures, respectively. This has been solved for a number of different laminates and the results are summarized in Table 1 and Fig. 3. The maximum relative difference $(1 - \lambda)$ has magnitudes as high as $\pm 8\%$ and is weakly dependent on the laminate layup. As can be seen in Fig. 3, the extremal deviations for regular symmetric angle-ply laminates occur in pairs for which the corresponding displacements are in-plane and out-of-plane, respectively. Although the state of strain is not constant over α, it can be characterized approximately as equal biaxial strain/curvature, pure shear/twist, and unequal biaxial strain/curvature for the upper, middle, and lower pairs of curves of Fig. 3, respectively. Similar trends were observed for the layups given in Table 1.

IV. Conclusions

The damping capacity of fiber-reinforced composite laminates has been calculated for general states of strain using the complex modulus approach and an alternative approach based on the components of the strain energy. It has been shown that the formulations are inconsistent with each other, although for the case of uniaxial stress the calculated differences are negligible. For more general states of strain, maximum discrepancies of approximately $\pm 8\%$ were found for a wide range of (carbon-epoxy) laminates. The discrepancy in any particular case is strongly dependent on the laminate configuration and the state of strain.

References

[1]Schapery, R. A., "Viscoelastic Behavior and Analysis of Composite Materials," *Mechanics of Composite Materials,* Vol. 2, Academic, New York, 1974, pp. 85–168.

[2]Jones, R. M., *Mechanics of Composite Materials,* Hemisphere, New York, 1975.

[3]Schultz, A. B., and Tsai, S. W., "Measurements of Complex Dynamic Moduli for Laminated Fiber-Reinforced Composites," *Journal of Composite Materials,* Vol. 3, July 1969, pp. 434–443.

[4]Gibson, R. F., and Plunkett, R., "Dynamic Mechanical Behavior of Fiber-Reinforced Composites: Measurement and Analysis," *Journal of Composite Materials,* Vol. 10, Oct. 1976, pp. 325–341.

[5]Ungar, E. E., and Kerwin, E. M., "Loss Factors of Viscoelastic Systems in Terms of Energy Concepts," *Journal of the Acoustical Society of America,* Vol. 34, No. 7, 1962, pp. 954–957.

[6]Adams, R. D., and Bacon, D. G. C., "Effect of Fiber Orientation and Laminate Geometry on the Dynamic Properties of CFRP," *Journal of Composite Materials,* Vol. 7, Oct. 1973, pp. 402–428.

[7]Saravanos, D. A., and Chamis, C. C., "Unified Micromechanics of Damping for Unidirectional and Off-Axis Fiber Composites," *Journal of Composites Technology and Research,* Vol. 12, No. 1, 1990, pp. 31–40.

[8]Hwang, S. J., and Gibson, R. F., "The Effects of Three-Dimensional States of Stress on Damping of Laminated Composites," *Composites Science and Technology,* Vol. 41, No. 4, 1991, pp. 379–393.

[9]Tschoegl, N. W., *The Phenomenological Theory of Linear Viscoelastic Behavior,* Springer-Verlag, New York, 1989, p. 454.

[10]Morison, W. D., "The Effects of Moisture Loss and Elevated Temperature upon the Material Damping of Fiber Reinforced Polymer Matrix Composites," Inst. for Aerospace Studies, Univ. of Toronto, Rept. 324, Ontario, Canada, July 1988.

Separated High Enthalpy Dissociated Laminar Hypersonic Flow Behind a Step—Pressure Measurements

S. L. Gai*
University of New South Wales, Australian Defence Force Academy, Campbell, ACT 2600, Australia

Introduction

THE impetus for the current resurgence of interest in hypervelocity flows is the increased activity in the area of space technology such as the reusable space planes, for example, the National Aero-Space Plane or NASP (United States), the HOTOL (United Kingdom), the HERMES (France), and the SÄNGER (Germany).

The design and development of these space vehicles, which operate at high velocity and high altitudes, make it imperative that detailed knowledge of the flowfield around such bodies is known. However, such data are still sparse, especially with respect to separating and reattaching flows. The separating and reattaching flow phenomenon is important because it may affect the control effectiveness and maneuverability of the vehicle or the propulsion/instrumentation unit may be located in the lee of the vehicle (e.g., the aeroassist flight experiment vehicle).

During the sixties a number of analytical and experimental separated and wake flow studies at both supersonic and hypersonic speeds were conducted.[1-7] These studies provided detailed insight and understanding into the behavior of separated flows with the separating boundary layer either laminar or turbulent. However, they dealt with only undissociated perfect gas with $\gamma = 1.4$. Not much information is available, therefore, pertaining to the behavior of separated flow at hypervelocities and under high enthalpy conditions at which the proposed space vehicles will operate.

In a recent study, Gai et al.[8] investigated laminar separated flow behind a two-dimensional backward-facing step in dissociated high enthalpy hypervelocity stream using a free-piston driven shock tunnel (FPST) that generates velocities and enthalpies experienced during the flight of aeroassisted space transfer vehicles (ASTVs). In that study, measurement of heat transfer and flow visualization using Mach-Zehnder interferometry were made and the importance of flow geometry and Reynolds numbers investigated. In the present Note, we describe pressure measurements made with the same model under similar flow conditions. To the author's knowledge, no data obtained under such high enthalpy hypervelocity flow conditions are currently available. This study is thus complementary to that described in Ref. 8.

Experiments

The experiments were conducted in the Australian National University free-piston driven shock tunnel T3[9] that can generate stagnation enthalpies and temperatures in air equivalent to those experienced by ASTVs. Under those conditions, dissociation of oxygen and nitrogen molecules can occur. The dissociated test gas in the reservoir at the end of the shock tube that is in chemical equilibrium and vibrationally fully excited is expanded through a hypersonic nozzle. As the gas expands through the nozzle, vibrational de-excitation and chemical

Received May 20, 1991; revision received Sept. 20, 1991; accepted for publication Nov. 1, 1991.

*Senior Lecturer, Mechanical Engineering Department, University College. Associate Fellow AIAA.

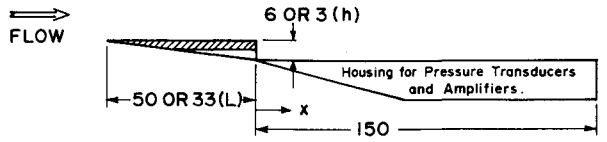

Fig. 1 Step model (all dimensions in mm).

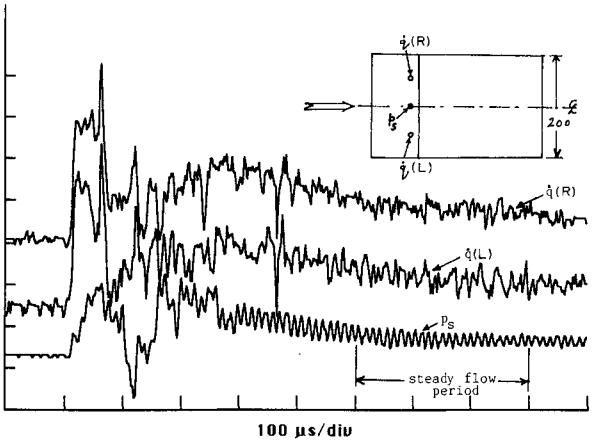

Fig. 2 Pressure and heat transfer traces just upstream of the step. The horizontal scale is time, 100 μs/div.; the vertical scale is heat transfer $\dot{q}$ 10 W/cm²/div; pressure p_s 10^{-3} bar/div.

recombination occur within the nozzle. However, not far downstream of the throat, the density and temperature become so low that those de-excitation and recombination processes "freeze" so that, at the exit of the nozzle, the freestream is a frozen nonequilibrium dissociated flow to which the model is exposed. Full details of chemical freezing in a hypersonic nozzle may be found, for example, in Ref. 10.

In the present investigation, the experiments were conducted at three flow conditions as summarized in Table 1. It will be noted from Table 1 that the Reynolds numbers are low enough so that the separating boundary layer is laminar under all test conditions.

The back step model consisted of an upstream flat plate L with a sharp leading edge and a step at the trailing edge, followed by a flat plate about 150 mm long. The step height was adjustable (6 or 3 mm), and depending on this, the upstream flat plate length was either 50 or 33 mm. The width of the model was 200 mm. The schematic of the model is shown in Fig. 1.

To make pressure measurements, Kulite semiconductor pressure transducers (series XCS-093, sensitivity 36 mV/psi) were positioned along the centerline of the rear flat plate, closely positioned in the vicinity of the step (typically 5 mm apart) but spaced further apart downstream. A pressure transducer was also located 3 mm upstream of the step, and the pressure measured by this transducer (p_s) was used as a reference pressure for normalizing the data. In addition, on the upstream flat plate, two coaxial surface thermocouples, also 3 mm upstream but on either side of the centerline and displaced 50 mm from it, were positioned. The results from those were used to check the two-dimensionality of the flow.[8] Because of the availability of a limited number of pressure transducers, no direct measurements of the base pressure p_b were made nor pressure transducers used to check the two-dimensionality of the flow. Figure 2 shows typical traces of heat transfer and pressure obtained upstream of the step. It is seen that the flow in the midspan region is reasonably two dimensional, and the output from the two thermocouple signals differs by no more than 20% during the steady flow period. The slight ringing seen on the pressure transducer signal is due to the impulsive aerodynamic loading during starting processes.

After pressure measurements were completed, some infinite fringe interferograms, using a Mach-Zehnder interferometer, were obtained as supplementary to the pressure data.

Results and Discussion

Figure 3 shows pressure distributions behind the step obtained with the two step heights and at the three flow conditions referred to in Table 1. The presures are normalized with respect to the pressure just ahead of the step (p_s) and the distances behind the step with respect to the step height. This method has generally been adopted oin the analysis of data of separated flow behind a step, for example, Roshko and Thomke.[5] It may be noted that the reference pressure p_s was slightly lower (5–10%) than the freestream static pressure p_∞ for the flow conditions. That is thought to be the result of the upstream influence of the corner expansion through the boundary layer δ_s at the corner, which for hypersonic flows would be quite strong.[7] Even at supersonic Mach numbers, Roshko and Thomke[5] have observed that effect.

The pressure distributions show the following features. First, for increasing values of δ_s/h (smaller step height), the pressure gradients are smaller and (extrapolated) base pressures (p_b) higher. This result is consistent with the observations of Charwat et al.[1] and Roshko and Thomke.[5] Second, sufficiently downstream, $x/h > 10$, the pressure overshoots by up to about 30% of the freestream value. The data points are insufficient to show clearly that the pressures attain the freestream values eventually. However, one can still discern the tendency for them to do so, especially in the case of the smaller step height. Such an overshoot has also been observed by Roshko and Thomke[5] but for larger step heights and lower Mach numbers. They attribute this to lack of two-dimensionality. Although we observe this discrepancy for the smaller step height, it is, however, possible that the flow in this region is affected by three-dimensional effects such as spillage from

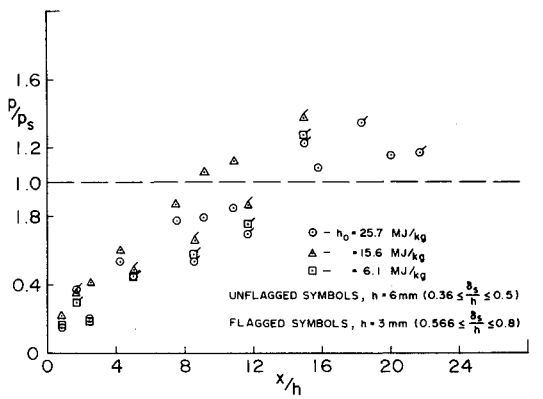

Fig. 3 Pressure distributions behind the step.

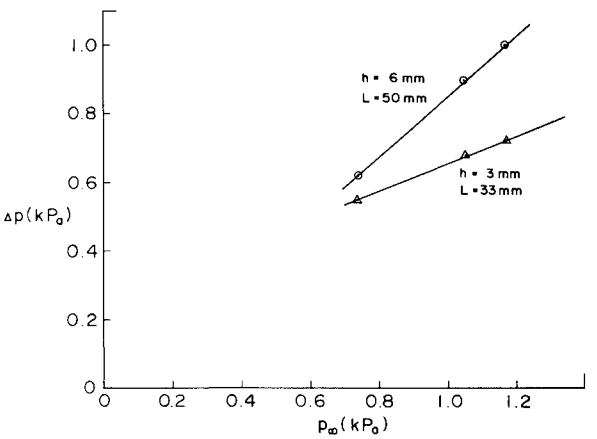

Fig. 4 Variation of Δp with freestream pressure.

Table 1 Test conditions at the exit plane of the nozzle

Stagnation conditions			Freestream conditions			
Pressure p_0, atm	enthalpy h_0, MJ/kg	equil. temp. T_0 K	Velocity v_∞ km/s	Density $\rho_\infty \times 10^3$, kg/m^3	Mach no., M_∞	Reynolds no. per met. length, m^{-1}
182	25.7	9315	6.23	2.13	7.1	7.37×10^4
180	15.6	7670	4.97	3.36	7.6	10.1×10^4
162	6.1	4285	3.29	6.4	8.1	19.1×10^4

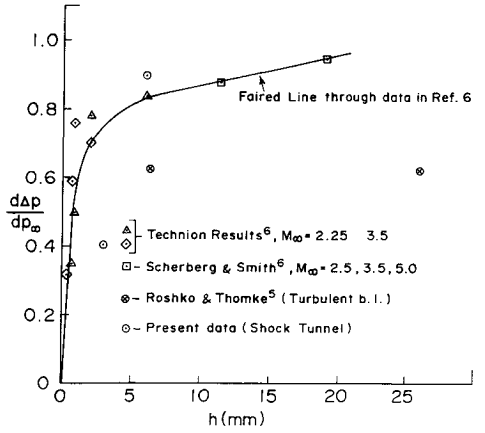

Fig. 5 Parameter ($d\Delta p/dp_\infty$) vs the step height.

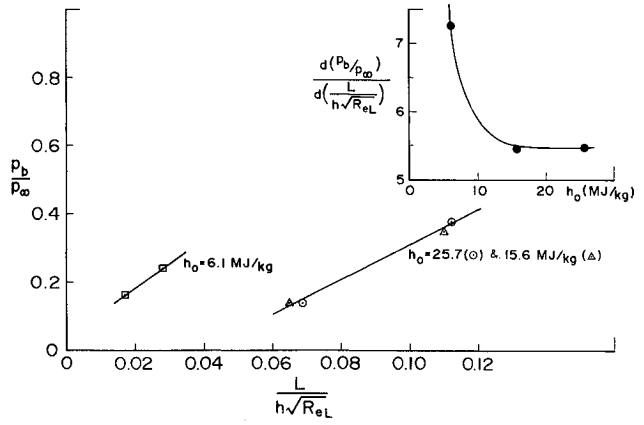

Fig. 6 Base pressure ratio vs the parameter ($L/h\sqrt{Re_L}$).

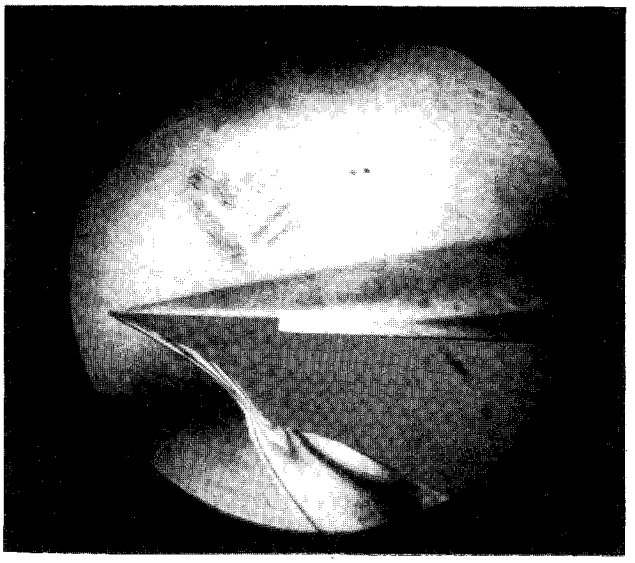

Fig. 7 Infinite interferogram of flow behind a step ($h = 3$mm; $h_0 = 15.1$ MJ/kg.

below because of a large wedge-shaped housing underneath the plate where electrical leads and amplifiers were located. This would cause higher pressures on the underside that in the absence of end plates might have affected the measurements.

A possibility as to whether this was a real gas effect was considered. However, this can be discounted for the following reasons. First, the flow is frozen upstream of step[8] and will remain frozen after expansion at the corner. Second, although it undergoes a compression through the wake shock, the recompression is weak and the recombination will not be strong enough to influence the pressures in any significant way.

Scherberg and Smith[6] show that there is a linear relationship between Δp ($=p_\infty - p_b$) and p_∞ for a given step height. This is found to be true also for the data of Roshko and Thomke[5] as well as the present data. In Fig. 4, in calculating Δp for the present measurements, extrapolated base pressure values from Fig. 3 have been used. Figure 5 shows the parameter ($d\Delta p/dp_\infty$) plotted against the step height in the manner of Scherberg and Smith. The data of Scherberg and Smith as well as the Technion data, as presented in Ref. 6, are also shown. We make the following observations. First, the Technion data and the present shock tunnel data (both of which were obtained at small step heights) fall in the region of rapid increase of ($d\Delta p/dp_\infty$) with h and, second, where ($d^2\Delta p/dp_\infty dh$) is changing. On the other hand, the data of Scherberg and Smith, which were obtained with larger step heights, seem to show ($d^2\Delta p/dp_\infty dh$) $\approx$ const and independent of Mach number. The data of Roshko and Thomke[5] seem to fall in an entirely different pattern, which may be due to the fact that in their experiments the boundary layer was turbulent and the configuration axisymmetric.

For a laminar boundary layer, $\delta_s \sim L/Re_L^{1/2}$ where $Re_L^{1/2}$ is the Reynolds number based on freestream conditions and the upstream plate length L. Then the scaling parameter δ_s/h for the flow behind the step becomes $L/h\sqrt{Re_L}$. Figure 6 shows the base pressure plotted against the parameter $(L/h\sqrt{Re_L}$. We note that, for a given enthalpy, increasing the Reynolds number decreases the base pressure, and this change seems to be more gradual for the higher enthalpy (nonequilibrium dissociated) flows (see inset).

Figure 7 is a typical infinite fringe interferogram of the flow behind the step. We clearly see the leading-edge shock wave, the boundary layer on the upstream flat plate, the shear layer behind the step, and the emergence of the reattachment shock. The reattachment shock seems to emerge from within the shear layer between 8–10 step heights. Notice the thick parallel shear layer that extends far downstream.

Conclusions

The study has shown that general features of hypervelocity laminar dissociated flow behind a step are qualitatively similar to those of an undissociated flow at moderate Mach numbers. However, the distinguishing feature of the present flow is the thick shear layer behind the step that shows very little curvature. Those features result in a gradual rise in pressure behind the step, especially postreattachment.

Acknowledgment

Thanks are due to W. Joe for his assistance during the experiments and data acquisition.

References

[1]Charwat, A. F., Roos, J. N., Dewey, C. F., and Hitz, J. A., "An Investigation of Separated Flow—Part I: The Pressure Field," *Journal of Aerospace Sciences*, Vol. 7, No. 6, 1961, pp. 457–470.

[2]Rom, J., and Seginer, A., "Laminar Heat Transfer to a Two-Dimensional Backward Facing Step from High Enthalpy Supersonic Flows in the Shock Tube," *AIAA Journal*, Vol. 2, No. 2, 1964, pp. 251–255.

[3]Reeves, B. L., and Lees, L., "Theory of Laminar Near Wake of Blunt Bodies in Hypersonic Flow," *AIAA Journal*, Vol. 3, No. 10, 1965, pp. 2061–2074.

[4]Weiss, R. F., and Weinbaum, S., "Hypersonic Boundary Layer Separation and the Base Flow Problem," *AIAA Journal*, Vol. 4, No. 5, 1966, pp. 1321–1330.

[5]Roshko, A., and Thomke, G. J., "Observations of Turbulent Reattachment Behind an Axisymmetric Downstream-Facing Step in Supersonic Flow," *AIAA Journal*, Vol. 4, No. 6, 1966, pp. 975–980.

[6]Scherberg, M. G., and Smith, H. E., "An Experimental Study of Supersonic Flow over a Rearward Facing Step," *AIAA Journal*, Vol. 5, No. 2, 1967, pp. 51–56.

[7]Hama, F. R., "Experimental Studies on the Lip Shock," *AIAA Journal*, Vol. 6, No. 2, 1968, pp. 212–219.

[8]Gai, S. L., Reynolds, N. T., Ross, C., and Baird, J. P., "Measurements of Heat Transfer in Separated High Enthalpy Dissociated Laminar Hypersonic Flow Behind Step," *Journal of Fluid Mechanics*, Vol. 199, Jan. 1989, pp. 541–561.

[9]Stalker, R. J., *Free Piston Shock Tunnel T3-Facility Hand Book*, Univ. of Queensland, Brisbane, Australia, 1985.

[10]Park, C., *Non Equilibrium Hypersonic Aerothermodynamics*, Wiley, New York, 1990, pp. 246–251.

New Method of Swirl Control in a Diffusing S-Duct

P. F. Weng* and R. W. Guo†
Nanjing Aeronautical Institute,
Nanjing 210016, People's Republic of China

Introduction

S-SHAPED intakes have been widely used in aircraft design. The investigation of curved ducts has received much attention. Previous papers by Guo and Seddon[1,2] show that the bulk vortex occurs because of flow separation at the bottom wall near the throat of the duct, which results in a large swirl (i.e., rotational flow) at the engine face. The swirl will get stronger when the separation region becomes larger.

The purpose of the swirl investigation in an S-duct is to control or curb the swirl. In Refs. 1 and 2, the solid spoiler, blocking of 15% of entry width from the inside wall, reverses the sense of the final swirl. Stocks and Bussiger[3] give swirl measurements for the tornado intake at 20-deg incidence for Mach 0.7 and at 3-deg incidence for Mach 1.8; the results also show the swirl reduction obtainable by the use of duct and curl fences. The authors[4] present a new approach called the vortex reduced device (VRD) method to control the swirl and to improve the average total pressure coefficient in an S-duct. The bulk vortex at the exit can be diminished to a smaller region. In Seddon's paper,[5] the sensitivities of swirl to fences are reported. In Vakili et al.'s paper,[6] an airfoil vortex device and flow control rail are used to reduce a pair of contrarotating vortices in the flow after the second bend. Lin and Guo[7] describe a vortex control device that decreases the swirl with increasing suction and even eliminates the bulk vortex if the suction is large enough.

Received Dec. 19, 1990; revision received Aug. 6, 1991; accepted for publication Aug. 12, 1991.

*Ph.D. Candidate, Aeroengine Department, P.O. Box 146.
†Professor, Vice President.

A new swirl control method, called the automatic adjustable blade (AAB) method, is described in this Note.

Experimental Description

An S-shaped diffuser was used, as shown in Figs. 1, consisting of five parts: lip, first bend, straight midsection, second bend, and straight rear section. The diffusser area ratio (exit area to throat area ratio) is 1.3095. Figures 1 also show the AAB device and its location on the model. The AAB has a NACA 0012-series profile, 110 mm long and 50 mm wide,

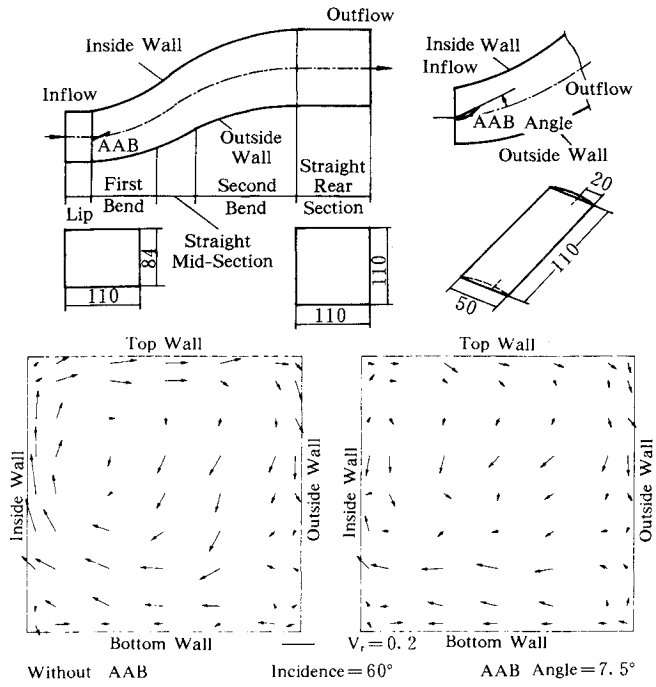

Fig. 1 Experimental model and exit velocity field.

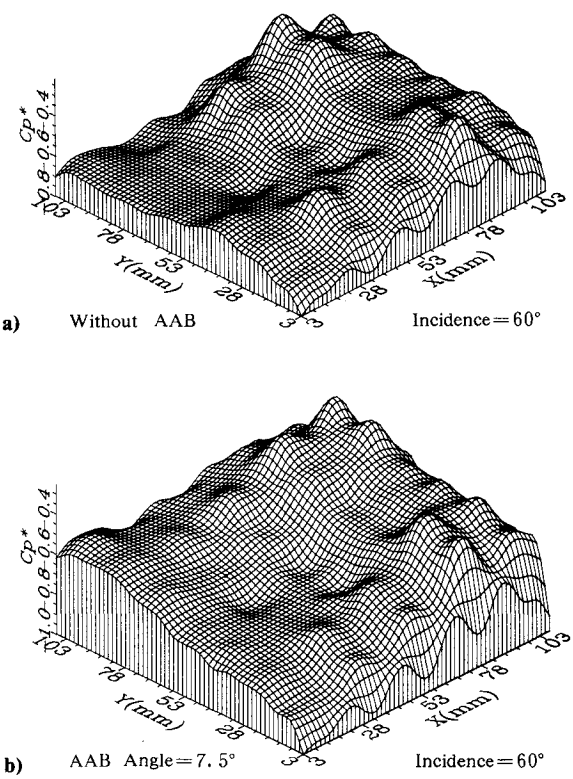

Fig. 2 Total pressure coefficient map: a) without AAB, incidence = 60 deg; b) AAB angle = 7.5 deg, incidence = 60 deg.